

Numerical simulation of the bifurcation-remerging process and intermittency in an undriven direct current glow discharge

Zijia Chu *School of Physics, Harbin Institute of Technology, Harbin 150001, People's Republic of China*Jingfeng Yao ,* Chengxun Yuan ,† Zhongxiang Zhou, Anatoly Kudryavtsev , Xiaou Wang, and Ying Wang*School of Physics, Harbin Institute of Technology, Harbin 150001, People's Republic of China**and Heilongjiang Provincial Key Laboratory of Plasma Physics and Application Technology, Harbin 150001, People's Republic of China*

(Received 10 October 2022; accepted 28 November 2022; published 21 December 2022)

As a complex nonlinear medium, gas discharge plasma can exhibit various nonlinear discharge behaviors. In this study, in order to investigate the chaos phenomenon in the subnormal glow region of an undriven direct current glow discharge, a two-dimensional plasma fluid model is established coupled with a circuit model as a boundary condition. Using the applied voltage as control parameter in the simulation, the complete period-doubling bifurcation and inverse period-doubling bifurcation processes in the oscillation region are found, and the influence of the applied voltage on the spatiotemporal distribution of plasma parameters during the bifurcation-remerging process is examined. In addition, the spatial distribution of the plasma parameters of the bifurcation-remerging process is also examined. Also, a series of periodic windows are present in the chaotic region, where the positions and relative order are generally consistent with the universal sequence. Additionally, this study showed that the intermittent chaos appears near the period-3 window, and the bursts appearing in the approximate periodic motion becomes more and more frequent as the control parameters move away from the saddle-node bifurcation point, which shows the typical type-I intermittent chaos characteristics.

DOI: [10.1103/PhysRevE.106.065207](https://doi.org/10.1103/PhysRevE.106.065207)

I. INTRODUCTION

In recent years, gas discharge plasma technology has been advancing relatively rapidly, and the low-temperature plasma generated by gas discharge has many important applications in the fields of material modification [1], waste water and gas treatment [2], sterilization and disinfection [3,4], thin film growth [5], nanopowder preparation [6], plasma display [7] and [8]. It has significant research value and far-reaching research prospects and its good economic benefits have gradually become apparent.

Among all the low-temperature plasma generation methods, direct current (dc) glow discharge is one of the earliest studied and most widely used methods [9]. In industrial production and daily applications, plasma stability is often required. However, as a highly nonlinear medium, gas discharge plasma often exhibits many complex nonlinear behaviors due to complex internal interactions [10–12]. The study of nonlinear phenomena in gas discharge plasma contributes to our understanding of the plasma discharge process with the aim of eventually controlling chaos in low-temperature plasma [13–15]. In addition, it is also important for research on relaxation oscillators in the fields of electronic circuits and neurodynamic [16], etc. Since the first observation of period-doubling bifurcation and chaos in helium dc glow discharge

plasma by Braun *et al.* [17], motivated many researchers to investigate the nonlinear phenomena occurring in gas discharge plasma with the aim of finding other routes to chaos in gas discharge plasma [18–20]. Researchers have achieved significant progress in the nonlinear dynamic behavior of gas discharge plasma for a variety of discharge structures. Numerous spatiotemporal nonlinear phenomena have been observed in laboratory plasmas, from dc glow discharge [21–27], dielectric-barrier discharge (DBD) [28–31], gas discharge-semiconductor system (GDSS) [10,32], and plasma jet [33], which involve self-pulses, self-organization, period-doubling bifurcation, intermittency, homoclinic bifurcation, and chaos. At present, it is believed that the nonlinear phenomena in gas discharge plasma are mainly due to the plasma operating in the negative differential conductivity section of the discharge current-voltage characteristic (CVC) curve [34]. Although outstanding achievements in the study of the complexities of gas discharge plasma have been made, most previous studies only go as far as describing experimental phenomena. Due to the limitation of measurement accuracy and the inevitable influence of noise, some discharge phenomena have not been consistently and reasonably explained, and the variation of discharge modes with external control parameters is not entirely clear.

In this study, a two-dimensional (2D) plasma fluid model is established to study the time-domain oscillation phenomena between the Townsend discharge region and the glow discharge region, coupling the external circuit into the model as a boundary condition. The entire process of mode transition is

*yaojf@hit.edu.cn

†yuancx@hit.edu.cn

demonstrated using applied voltage as the control parameter. The results showed that, with the increase of applied voltage, the discharge will undergo a transition from regular periodic oscillations to chaos via period-doubling bifurcation, and then return to periodic oscillations via an inverse period-doubling bifurcation process. The results are in good agreement with the experimental observations contained in Refs. [21,22]. The article is organized as follows. After this introduction, the governing equations and the boundary conditions are given in Sec. II. Then, the calculation results and discussion are presented in Sec. III and finally the conclusions drawn from the simulations are summarized in Sec. IV.

II. MODEL

A. Governing equations

The simulation is based on the fluid model, solved to obtain the spatial distribution of the particle number density, electron energy density, and electric potential. Argon is used as the working gas since it has simple chemical reactions and has been extensively investigated.

The particle density of different species (electrons, excited atoms and ions) n_k is determined by the particle number balance equation,

$$\frac{\partial n_k}{\partial t} + \nabla \cdot \mathbf{\Gamma}_k = S_k, \quad (1)$$

where S_k represents the source term due to the collision reaction, the particle flux $\mathbf{\Gamma}_k$ under the drift-diffusion approximation has the form,

$$\mathbf{\Gamma}_k = -\mu_k n_k \mathbf{E} - D_k \nabla n_k, \quad (2)$$

The electron energy density n_ε is determined using the electron energy conservation equation,

$$\frac{\partial n_\varepsilon}{\partial t} + \nabla \cdot \mathbf{\Gamma}_\varepsilon = -e \mathbf{\Gamma}_e \mathbf{E} + S_\varepsilon, \quad (3)$$

where the first term on the right-hand side represents the Joule heat source and the second term indicates the increased energy due to the collision. The relationship between the electron energy density and the electron density can be expressed as $n_\varepsilon = n_e \bar{\varepsilon}$, where $\bar{\varepsilon} = 3/2k_B T_e$ is the mean electron energy, and the energy flux $\mathbf{\Gamma}_\varepsilon$ can be expressed as

$$\mathbf{\Gamma}_\varepsilon = -\mu_\varepsilon n_\varepsilon \mathbf{E} - D_\varepsilon \nabla n_\varepsilon, \quad (4)$$

the electric potential φ is determined by the Poisson equation,

$$-\varepsilon_0 \nabla^2 \varphi = \sum_k q_k n_k, \quad \mathbf{E} = -\nabla \varphi. \quad (5)$$

In the above equations, μ and D represent the mobility and diffusion coefficient, respectively. For electrons, the mobility μ_e and diffusion coefficients D_e are calculated from Eqs. (6) and (7),

$$\mu_e = -\frac{2e}{m} \int_0^{+\infty} \frac{\varepsilon}{3v_{ea}} \sqrt{\varepsilon} \frac{\partial}{\partial \varepsilon} f_0(\varepsilon) d\varepsilon, \quad (6)$$

$$D_e = \frac{2e}{m} \int_0^{+\infty} \frac{\varepsilon}{3v_{ea}} \sqrt{\varepsilon} f_0(\varepsilon) d\varepsilon, \quad (7)$$

where ε is the electron kinetic energy, v_{ea} is the momentum transfer frequency. In the fluid model, the electron energy

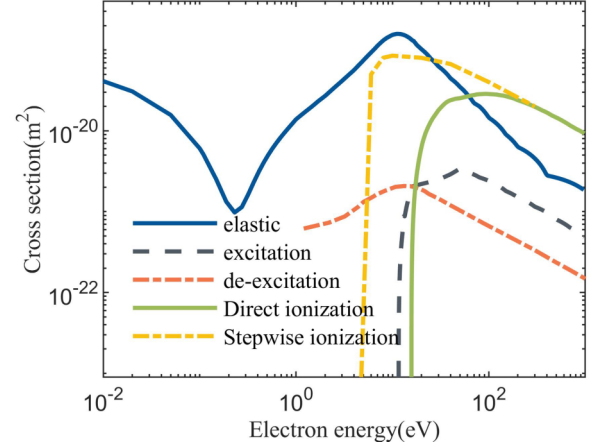


FIG. 1. Cross sections of chemical reactions in the model.

distribution function (EEDF) $f_0(\varepsilon)$ should be predefined. It is worth noting that although the use of different EEDFs can significantly affect the rate constants of the chemical reactions, at a macroscopic level it still gives qualitatively similar CVCs, which are of more interest to us. Therefore, it is assumed that in the simulation, the electrons follow the Maxwell distribution, which has proven to be feasible in the related experiments [9,35,36]. The relationships $\mu_\varepsilon = 5/3\mu_e$ and $D_\varepsilon = 5/3D_e$ are satisfied between the electron energy transport coefficient and the electron transport coefficient.

In the fluid model, the source terms S_k and S_ε in the above continuity equation are related to the chemical reactions involved in the plasma. In the model, neutral argon atoms, electrons, ions, and metastable state argon atoms are considered. The chemical reactions involved in the simulations are given in Table I, whose collision cross sections of the electron collision reactions are shown in Fig. 1. Thus, the source term S_k and S_ε can be expressed as,

$$S_e = S_i = k_2 n_0 n_e + k_5 n_m n_e + k_6 n_0 n_m, \quad (8)$$

$$S_m = k_3 n_0 n_e - k_4 n_e n_m - k_5 n_e n_m - 2k_6 n_m^2 - k_7 n_0 n_m, \quad (9)$$

$$S_\varepsilon = -3/2 \delta v_{ea} n_e k_B (T_e - T_g) + k_2 n_0 n_e \Delta E_2 + k_3 n_0 n_e \Delta E_3 + k_4 n_m n_e \Delta E_4 + k_5 n_m n_e \Delta E_5, \quad (10)$$

where n_0 is the density of neutral argon atoms, $\delta = 2m_e/m_g$, the background gas temperature $T_g = 300$ K, and k_n is the rate constant corresponding to the n th reaction, the cross section data is obtained from the Phelps database [37], and the relationship with the collision cross section is

$$k_n = \int_0^{+\infty} \sigma_n(\varepsilon) v(\varepsilon) \sqrt{\varepsilon} f_0(\varepsilon) d\varepsilon. \quad (11)$$

B. Boundary conditions

The normal flux of electrons and electron energy are given by

$$\mathbf{n} \cdot \mathbf{\Gamma}_e = \frac{1 - r_e}{1 + r_e} \left(\frac{1}{2} v_{e,th} n_e + n_e \mu_e (\mathbf{E} \cdot \mathbf{n}) \right) + \sum_i \gamma_i (\mathbf{\Gamma}_i \cdot \mathbf{n}) \quad (12)$$

TABLE I. Chemical reactions considered in the simulation.

Reaction	Type	$\Delta E(eV)$	Constant
$e + Ar \rightarrow e + Ar$	Elastic collision	0	Calculated from Eq. (11)
$e + Ar \rightarrow 2e + Ar^+$	Direct ionization	15.8	Calculated from Eq. (11)
$e + Ar \rightarrow e + Ar^*$	Excitation	11.5	Calculated from Eq. (11)
$e + Ar^* \rightarrow e + Ar$	Deexcitation	-11.5	Calculated from Eq. (11)
$e + Ar^* \rightarrow e + Ar^+$	Stepwise ionization	4.4	Calculated from Eq. (11)
$Ar^* + Ar^* \rightarrow e + Ar + Ar^+$	Penning ionization	-	Ref. [37]
$Ar^* + Ar \rightarrow Ar + Ar$	Metastable quenching	-	Ref. [37]

$$\mathbf{n} \cdot \mathbf{\Gamma}_e = \frac{1 - r_e}{1 + r_e} \left(\frac{5}{6} v_{e,th} n_e + n_e \mu_e (\mathbf{E} \cdot \mathbf{n}) \right) + \sum_i \gamma_i \bar{\epsilon}_i (\mathbf{\Gamma}_i \cdot \mathbf{n}) \quad (13)$$

where \mathbf{n} is the outer normal direction unit vector of the wall; $v_j = \sqrt{8k_B T_j / \pi m_j}$ ($j = e, i, m$) is the thermal velocity; γ is secondary electron emission coefficient, which is set to 0.25 in the model; $\bar{\epsilon}_i$ is the mean energy of secondary electrons. For positive ions, particle number loss due to migration should be considered, and the boundary condition is given by,

$$\mathbf{n} \cdot \mathbf{\Gamma}_i = 1/4 n_i v_i - \alpha n_i \mu_i (\mathbf{n} \cdot \mathbf{E}), \quad (14)$$

where the coefficient $\alpha = 1$ when $(\mathbf{n} \cdot \mathbf{E}) > 0$, otherwise $\alpha = 0$. For excited atoms, the boundary condition is as follows:

$$\mathbf{n} \cdot \mathbf{\Gamma}_m = 1/4 n_m v_m. \quad (15)$$

For the electric potential, consider the coupling of RC external circuit, we set $\varphi = 0$ at the cathode and $\varphi = U$ at the anode, which is satisfied by,

$$\frac{dU}{dt} + \frac{1}{C} \left(I - \frac{U_0 - U}{R} \right) = 0, \quad (16)$$

where U_0 is the total voltage, I is the total current, R is the ballast resistance, and C is the capacitance.

III. RESULTS AND DISCUSSION

A. Current-voltage curve

A dc gas discharge between two parallel electrodes in a vacuum tube is considered in this work. The length of the discharge tube is $L = 15$ cm, the radius is $R_0 = 1.25$ cm, and the electrode gap is $d = 7$ cm. The parameters of the RC external circuit are selected as $R = 10^6 \Omega$ and $C = 10$ pF. A 2D fluid model is built using the built-in plasma module in COMSOL MULTIPHYSICS software. The CVC curve for the discharge pressure $p = 40$ Pa, shown in Fig. 2, where the abscissa is presented in logarithmic scale, contains a rapidly declining negative slope section and a relatively flatter positive slope section, which allows us to consider the plasma as an electronic component with the current-controlled negative resistance characteristics. Multiple previous studies on nonlinear electronic circuits have suggested that a negative differential conductivity is required to cause self-sustained oscillations [38–40]. With the consideration of the coupling with the external circuits, the unstable oscillation will occur when the equilibrium point of the discharge, i.e., the intersection of

the load line $U = U_0 - IR$ and CVC $U = U(I)$, is in the blue dashed region in Fig. 2. The two sides of the oscillation region correspond to the stable Townsend discharge region and the glow discharge region, respectively. The present simulations find that under appropriate parameters, the undriven dc glow discharge system can show rich dynamical behaviors.

B. Evolution characteristics of dynamical behaviors

In this section, we present a detailed investigation of the mode transitions in the oscillation region. The solution in the stable glow discharge state is used as the initial condition for subsequent calculations, where the solution time is long enough so that eventually the system state will no longer change. The first and second rows in Fig. 3 show the evolution of the time-domain oscillations of the plasma voltage and current for the applied voltage $U_0 =$ (a) 205.1 V, (b) 210 V, (c) 212.6 V, and (d) 214 V. The third row displays the trajectory in the current-voltage phase space and the fourth row shows the return map $A_n \times A_{n+1}$ of the voltage waveform, where A_n is the n -th maximum of the voltage amplitude. The results in Figs. 3(a1)–3(a2) reveal that, since the applied voltage U_0 increases to a value slightly above its critical value of about 205 V, the equilibrium point will lose its stability and the system no longer converges to the stable state, instead, periodic oscillations around the equilibrium point will appear. The attractor in the phase space evolves into a limit cycle [as shown in Fig. 3(a3)], which indicates a Hopf bifurcation and a self-sustained oscillation of the system in the absence of an

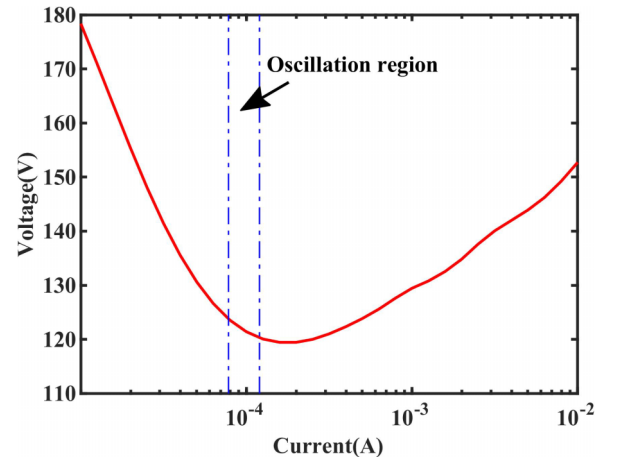


FIG. 2. Current-voltage characteristics of the discharge in argon, pressure is $p = 40$ Pa.

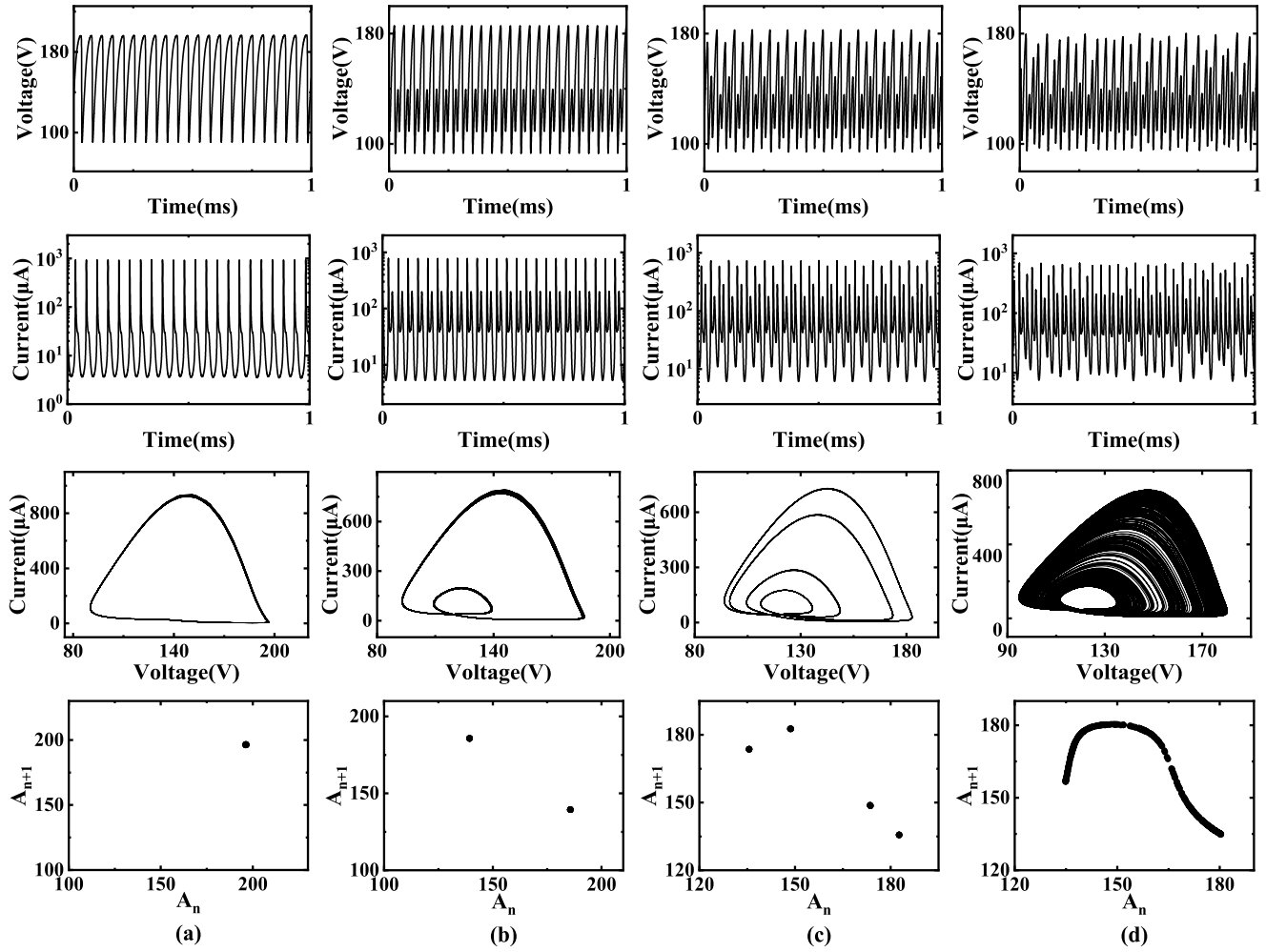


FIG. 3. Evolution of the time-domain oscillations of discharge voltage (first row), evolution of the time-domain oscillations of discharge current (second row), phase trajectory in current-voltage phase space (third row), and return map (fourth row) for different applied voltages $U_0 =$ (a) 205.1 V, (b) 210 V, (c) 212.6 V, (d) 214 V.

externally periodic forcing. From the number of loops of the limit cycle and the return map in Fig. 3(a4), it can be concluded that the system is in the period-1 oscillation mode. As U_0 continues to increase, a new phenomenon appears, as can be observed in Figs. 3(b1)–3(b4), in which the system undergoes a period-doubling bifurcation. In this case, each voltage and current pulse no longer maintains the same amplitude, instead a high-amplitude pulse is followed by a low amplitude pulse, with one oscillation period containing two pulses with different amplitudes. The phase diagram shows that a new loop is created from the previous limit cycle, so that the period of the new limit cycle is twice that of the old one. The data in the return map is almost concentrated at two points, indicating that the system switches from a period-1 oscillation mode to a period-2 oscillation mode, which means that the instability of the system increases as the control parameter U_0 increases. Further period-doubling bifurcation will occur at higher U_0 , as can be seen in Figs. 3(c1)–3(c2), where the voltage and current waveforms will contain four pulses of different amplitudes in one period at $U_0 = 212.6$ V. The phase diagram in Fig. 3(c3) and the return map in Fig. 3(c4) show that the system undergoes a transition from period-2 to period-4.

According to Feigenbaum’s theory, the parameter interval ΔU_0 between each period doubling occurrence will gradually decrease, and eventually the system will transition to a fully chaotic state after numerous period-doubling bifurcation. For $U_0 = 214$ V, it can be seen from Fig. 3(d1) and Fig. 3(d2) that the oscillation waveforms in the time-evolution diagrams of the current and voltage will be completely irregular, and the system will transition to a nonperiodic motion. In this case, the trajectories in the phase space will fill a certain area densely. In addition, it can be seen from the return map that the data are almost concentrated on a smooth single-peaked curve with extremely narrow width, which is almost identical to the return map obtained from a one-dimensional single-peaked mapping (e.g., logistic map), suggesting that the transition to the chaotic regime in the plasma occurs through a period doubling bifurcation, in keeping with the Feigenbaum’s theory.

Apparently, as U_0 continues to increase, the system will not sustain the chaotic state (which will transition to a stable glow discharge state at a sufficiently high applied voltage). The transition of the discharge from a chaotic state to a glow discharge state was investigated subsequently. The results show that in dc glow discharge systems there exists not only

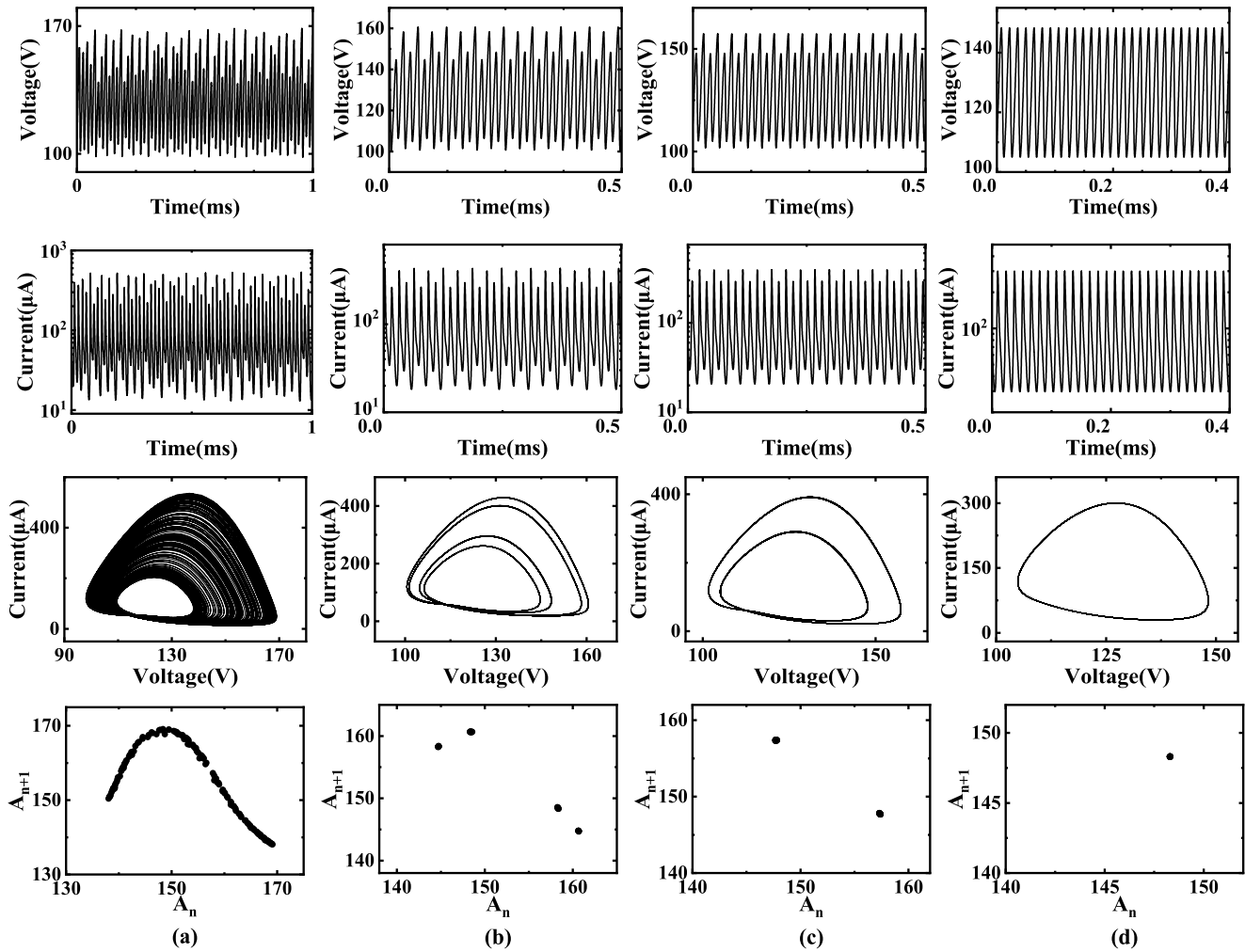


FIG. 4. Evolution of the time-domain oscillations of discharge voltage (first row), evolution of the time-domain oscillations of discharge current (second row), phase trajectory in current-voltage phase space (third row) and return map (fourth row) for different applied voltages $U_0 =$ (a) 218 V, (b) 219.8 V, (c) 220.5 V, (d) 223 V.

a bifurcation process from periodic oscillation state to chaos, but also a process of reforming an ordered oscillation state after chaos. Figure 4 shows the evolution of the time-domain oscillations for discharge voltages (first row) and discharge currents (second row), the trajectories in voltage-current phase space (third row) and the return map (fourth row) for applied voltages of $U_0 =$ (a) 218 V, (b) 219.8 V, (c) 220.5 V, and (d) 223 V, respectively. The transient processes at the initial moments are also neglected. It can be seen in Figs. 4(a1)–4(a4) and 4(b1)–4(b4), while U_0 is increased from 218 V to 219.8 V, the discharge transitions from a chaotic state with irregular oscillations to a periodic oscillation state, where each period contains four voltage (current) pulses of different amplitudes. Both the phase space trajectory and the return map indicate that the system transitions to a period-4 oscillation state. As the voltage increases further, the inverse period bifurcation process will be observed, and the transition to the period-2 and period-1 oscillation states can be obtained at $U_0 = 220.5$ V [Figs. 4(c1)–4(c4)] and $U_0 = 223$ V [Figs. 4(d1)–4(d4)]. Eventually, the discharge transitions to a stable glow discharge state once the applied voltage is above 224 V and the periodic oscillation disappears. From

the above analyses, as the control parameters are gradually increased, the process of period-doubling bifurcation and inverse period-doubling bifurcation will occur successively in the oscillation region, the discharge transitioned from regular periodic oscillation to irregular chaotic oscillation and then to regular periodic oscillation again, the system undergoes an order-chaos-order transition.

C. Global nonlinear dynamic characteristics

In order to briefly visualize the evolution of the oscillation mode, a bifurcation diagram is constructed as shown in Fig. 5(a), in which the data points represent local maxima in the voltage waveform. The detail enlargements of the left and right parts of the bifurcation diagram are shown in Fig. 5(b) and 5(c), respectively. The bifurcation diagrams shown in Figs. 5(a)–5(c) reveal that with the gradual increase of the control parameter, the system undergoes a transition from a periodic oscillation state to a chaos state through a typical period-doubling bifurcation route, and subsequently transitions back to regular periodic oscillations through an inverse period-doubling bifurcation route. The system has undergone

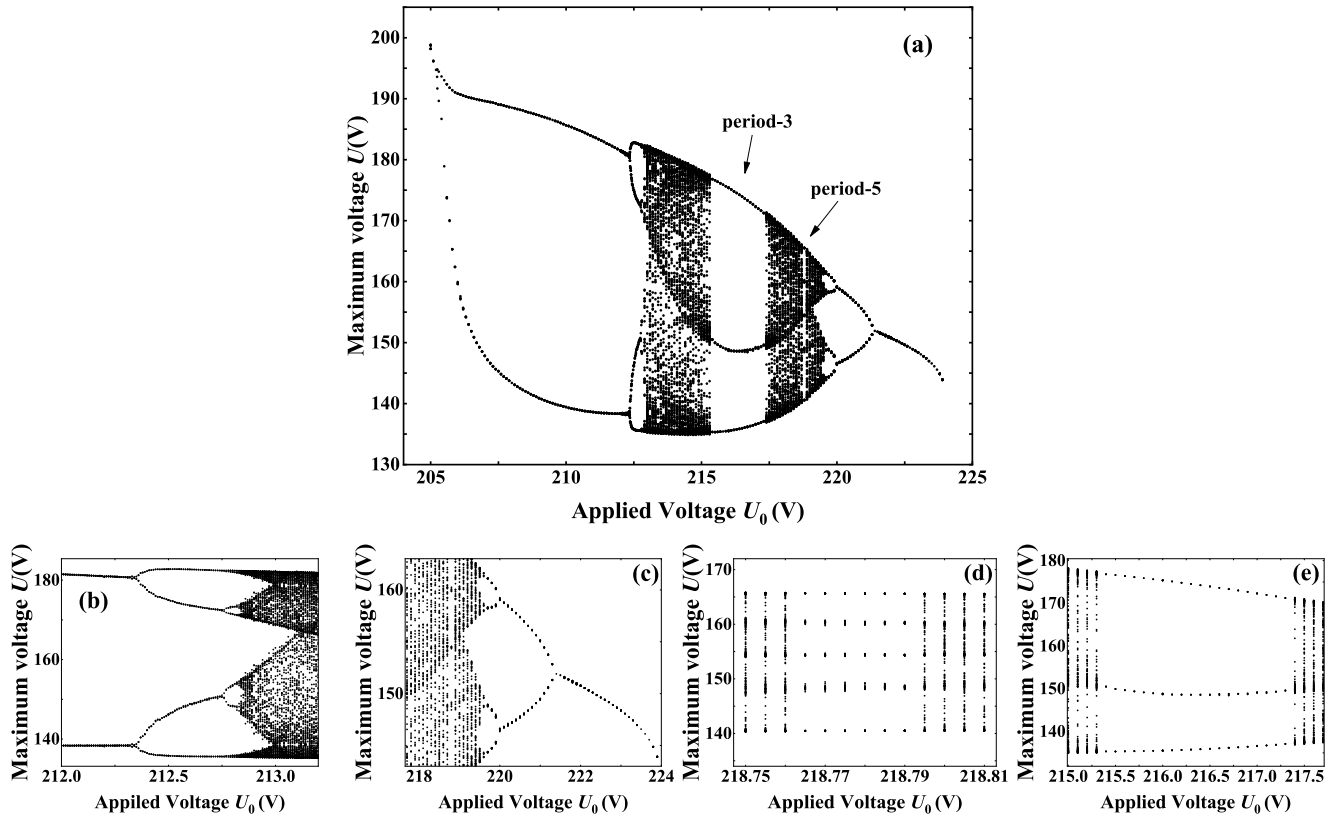


FIG. 5. (a) Amplitude bifurcation diagram. (b) Period-doubling bifurcation process. (c) Inverse period-doubling bifurcation process. (d) Period-5 window between 218.765 V and 218.79 V. (e) Period-3 window between 215.4 V and 217.3 V.

the bifurcation-remerging process. In addition, there is a fine structure within the chaotic region. As shown in the Fig. 5(a), there are several periodic windows within the chaotic region. Two distinct periodic windows are the period-3 and the period-5, respectively, which are indicated in the diagram in Fig. 5(a). The period-5 window occupies a relatively narrow parameter range, while the period-3 window occupies a wider parameter range and connects the period-doubling bifurcation process with the inverse period-doubling bifurcation process. The position and order of the periodic windows essentially correspond to the universal sequence of periodic orbits. According to the Li-Yorke theorem, the presence of the period-3 window means that arbitrary integer periods can be found, which implies that the system has an infinite self-similar structure. Magnified views of the period-3 and period-5 windows are shown in Fig. 5(d) and Fig. 5(e), respectively. The voltage waveforms for the period-5 oscillation mode ($U_0 = 218.79$ V) and the period-3 oscillation mode ($U_0 = 216.5$ V) are shown in Fig. 6(a) and Fig. 6(b), respectively. For the period-5 oscillation mode, five pulses of different amplitudes are contained in one period, while for the period-3 oscillation mode, one period contains three pulses of different amplitudes.

D. Spatial distribution of plasma parameters

To determine the plasma properties of the bifurcation-remerging process, the time-evolution curves of the discharge current for $U_0 = 205.1$ V (red line) and $U_0 = 223$ V (blue line) are depicted in Fig. 7(a). It can be seen that both curves

exhibit a period-1 oscillation and the period of oscillation becomes significantly shorter with higher voltage. Meanwhile, the duration of the current pulse does not increase significantly, which is the characteristic discharge time after the electrode gap is broken down. The axial spatial evolution curves of the electron density and electric potential for the two above-applied voltages, at the moments of the maximum current indicated by a circle and the minimum current indicated by a square in Fig. 7(a), are shown in Figs. 7(b) and 7(c). The spatial distribution at the moments of the maximum current for both applied voltages shows obvious characteristics of the glow discharge, as can be seen in Fig. 7(b). The cathode sheath region, which contains almost the entire potential drop, the negative glow region with the highest electron density and the positive column region where the electron density remains essentially constant are clearly visible. However, when the current is at a minimum, a clear difference in the spatial distribution appears. The dashed line in the Fig. 7(c) reveals that for $U_0 = 205.1$ V, the maximum of the electron density is only about 10^{11} m⁻³. Meanwhile, the quasineutral region is not formed and the spatial distribution of the electric potential is essentially undistorted. Thus, it can be concluded that the electrode gap has not yet breakdown and the discharge is in a typical Townsend discharge mode. Instead, for the condition of $U_0 = 223$ V, compared with $U_0 = 205.1$ V, the electron density and current are two orders and one order of magnitude higher, respectively. Meanwhile, the electric potential is somewhat distorted, with the potential drop starting to be concentrated near the cathode. At this condition, the system

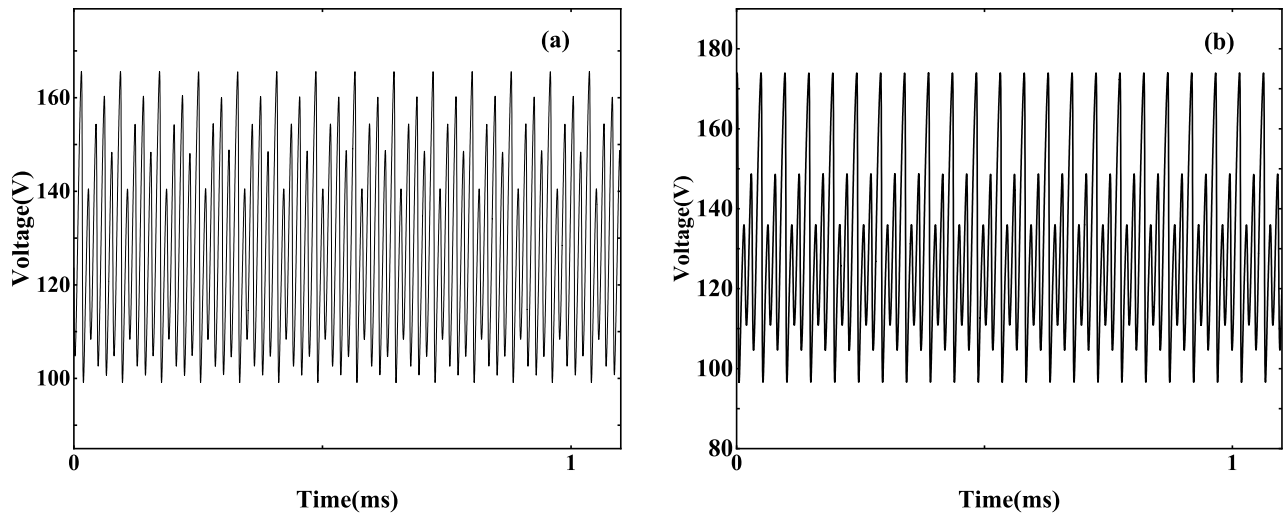


FIG. 6. (a) Voltage waveform in period-5 window, where $U_0 = 218.79$ V. (b) Voltage waveform in period-3 window, where $U_0 = 216.5$ V.

exhibits neither the characteristics of Townsend discharge nor glow discharge, and can be considered to be in the transition stage of both, i.e., a subnormal glow discharge mode. There-

fore, it can be concluded that for the unstable discharge at low applied voltage (bifurcation stage), the system transitions between the Townsend discharge mode and the glow discharge

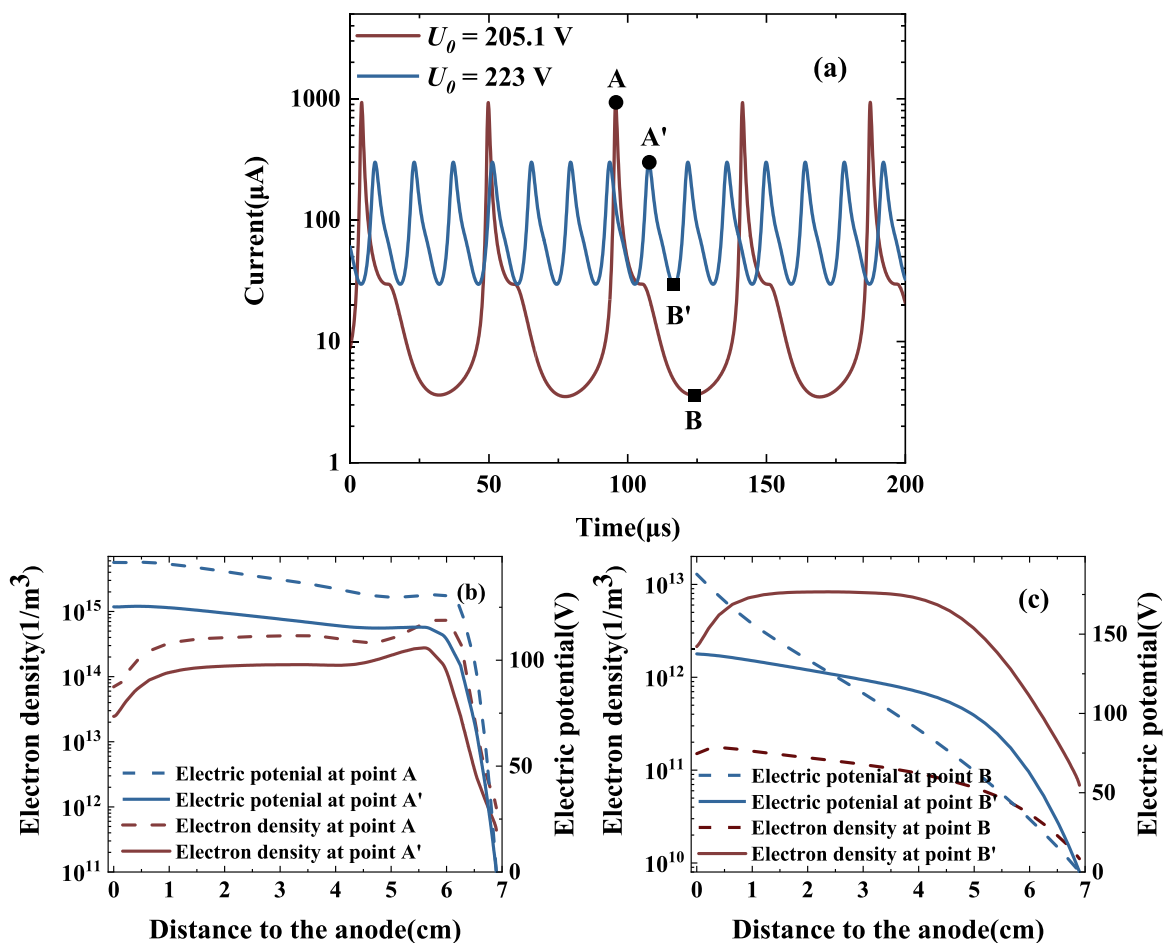


FIG. 7. (a) The temporal evolution curves of discharge current for $U_0 = 205.1$ V (red line) and $U_0 = 223$ V (blue line). (b) The axial spatial evolution curves of the electron density (red line) and electric potential (blue line) for $U_0 = 205.1$ V (dotted line) and $U_0 = 223$ V (solid line) at the moments of the maximum current indicated by a circle. (c) The axial spatial evolution curves of electron density (red line) and electric potential (blue line) for $U_0 = 205.1$ V (dotted line) and $U_0 = 223$ V (solid line) at the moments of the minimum current indicated by a square.

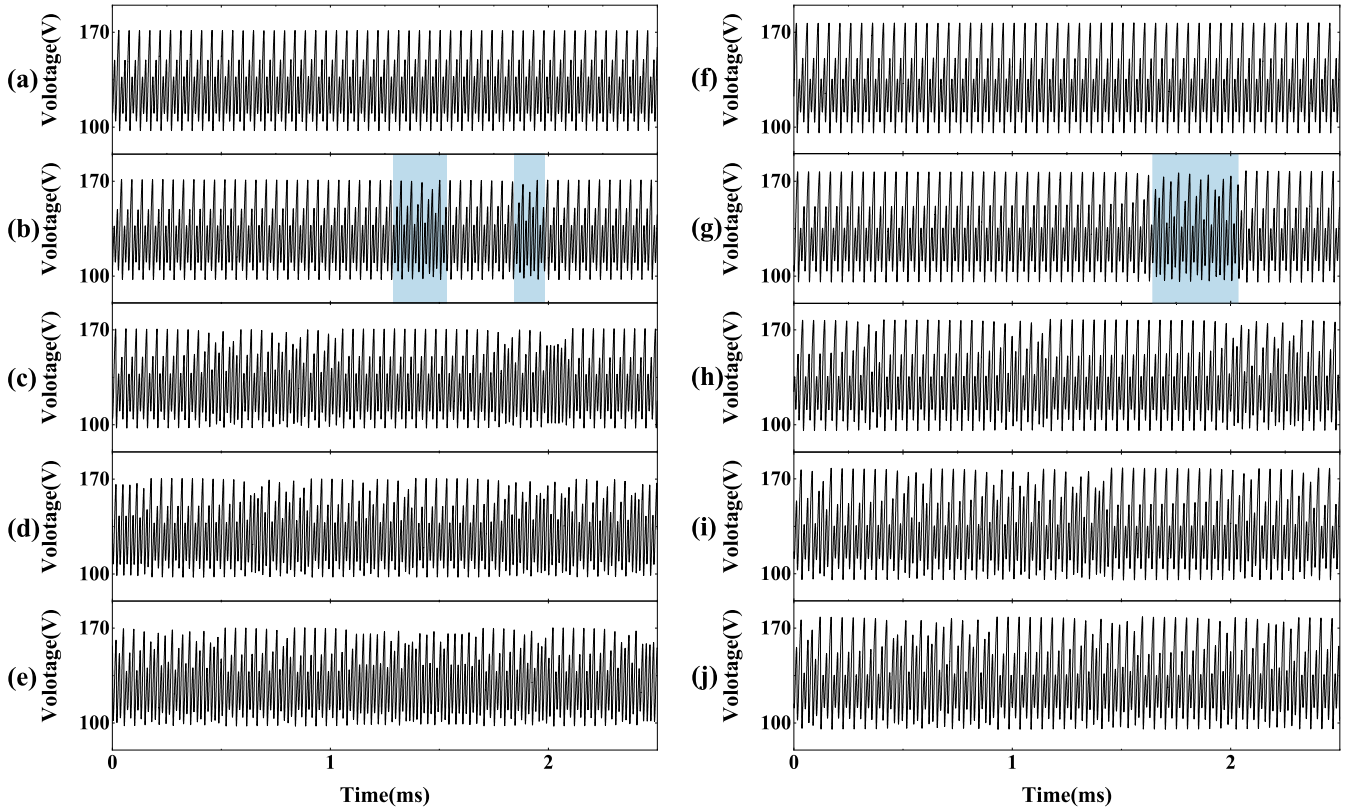


FIG. 8. Waveforms of discharge voltage at different applied voltages $U_0 =$ (a) 217.3 V, (b) 217.4 V, (c) 217.5 V, (d) 217.6 V, (e) 217.7 V, (f) 215.4 V, (g) 215.3 V, (h) 215.2 V, (i) 215.1 V, (j) 215 V.

mode, while for the high applied voltage (remerging stage), the system transitions between the subnormal glow discharge mode and the glow discharge mode.

E. Intermittent chaos near the periodic window

Another phenomenon is the presence of intermittent chaos near the periodic window. The voltage waveform on both sides of the period-3 window are illustrated in Fig. 8, where the parameters in Figs. 8(a)–8(e) are chosen to be $U_0 = 217.3\text{--}217.7$ V with a spacing of 0.1 V, while the parameters in Figs. 8(f)–8(j) are chosen to be $U_0 = 215.4\text{--}215$ V with a spacing of -0.1 V. The results in Figs. 8(a) and 8(f) reveal a stable period-3 oscillation similar to that in Fig. 6(b). When the applied voltage U_0 exceeds the critical value U_c , several occasional irregular bursts appear in the voltage waveform [e.g., in the blue area of Figs. 8(b) and 8(g)]. Beyond the irregular bursts the waveform still maintains an approximate period-3 oscillation state. The system is in a state that the regular and irregular oscillations alternate. As the voltage gradually moves away from the critical value, such irregular bursts will become more frequent and the proportion of approximate periodic oscillation will decrease, as shown in Figs. 8(c)–8(e) and 8(h)–8(j). Eventually, a transition to a fully chaotic regime can occur, which is typically characteristic of intermittent chaos.

The type-I intermittent chaos will occur near the critical point of the saddle-node bifurcation. The third-iteration map $A_n \times A_{n+3}$ for $U_0 = 217.7$ V is shown in Fig. 9(a), and the iterative process inside the gray dashed box is shown in

Fig. 9(b). It can be seen that when intermittent chaos occurs in the system, three narrow channels are formed between the third-iteration map and the diagonal. When the orbit enters the entrance of one of the narrow channels, it will require several iterations to leave the channel. Due to the narrow width of the channel, the iterations within the channel will be similar to that near the fixed point, satisfying $A_{n+3} \approx A_n$ [as shown by the red line in Fig. 9(b)], which corresponds to an approximate period-3 oscillation in the waveform (sometimes called laminar regions). As the iteration exits the channel, there are some dramatic, irregular jumps that correspond to irregular oscillating regions in the waveform (sometimes called turbulent regions) until it enters another narrow channel. The width of the channel is related to the distance of the control parameter U_0 from the critical value of the periodic window U_c : As $|U_0 - U_c|$ that gradually increases, i.e., the control parameter moves away from the periodic window, the width of the channel increases, indicating that fewer iterations are needed to escape from the channel; In contrast, as $|U_0 - U_c|$ gradually decreases, the width of the channel gradually decreases, corresponding to a gradual increase in the laminar width. Eventually the channel will intersect with the diagonal when $|U_0 - U_c|$ decreases to zero, and a pair of fixed points will appear due to the occurrence of saddle-node bifurcation. The unstable fixed points will degenerate during the iterative process, and the system will converge to the stable fixed point eventually, which is given in Fig. 9(b) for $U_0 = 217.3$ V. The saddle-node bifurcation leads to the appearance of the periodic window in the chaotic region.

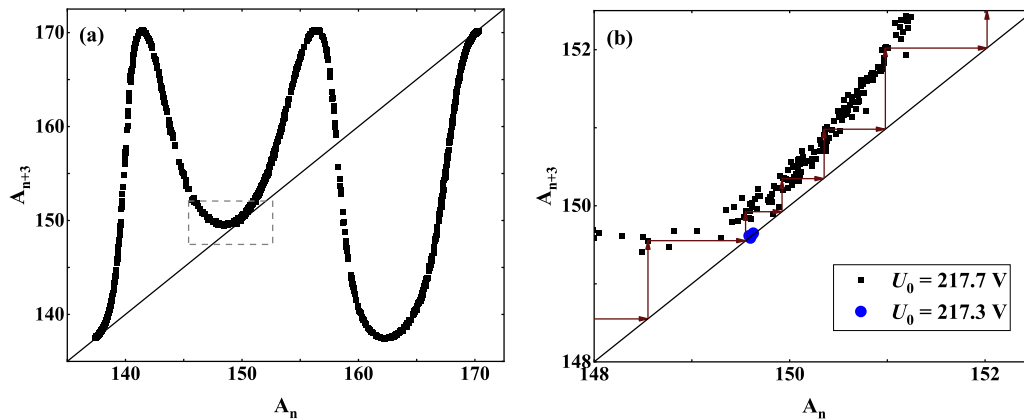


FIG. 9. (a) Third-iterate map for applied voltage $U_0 = 217.7$ V. (b) Iterative process inside the grey dashed box.

IV. CONCLUSIONS

In this study, we investigated the nonlinear dynamical behaviors of the dc glow discharge in the subnormal glow region by developing a 2D plasma fluid model coupled to external circuits through boundary conditions. The time-domain nonlinear discharge behaviors and its evolution under different control parameters (i.e., applied voltage) are investigated in-depth. The bifurcation-remerging phenomenon and the fine structure of chaos are found, which enriches and refines the time-domain nonlinear phenomena in an undriven dc glow discharge.

There is an oscillation region between the Townsend discharge region and the glow discharge region due to the negative differential conductivity. The results show that with the increase of the applied voltage, the discharge system occurs through a bifurcation-remerging process and undergoes an order-chaos-order transition at the given discharge parameters. The entire process that the discharge system undergoes as the applied voltage increases can be described as follows: a stable Townsend discharge, bifurcation-remerging process and stable glow discharge. For the bifurcation-remerging

process, the plasma parameter distribution is examined in depth. The results showed that for the bifurcation stage the plasma system transitions between the Townsend discharge mode and the glow discharge mode, while for the remerging stage the system transitions between the subnormal glow discharge mode and the glow discharge mode. In addition, several periodic windows within the chaotic region are present, and the existence of an inverse saddle-node bifurcation near the critical value of the periodic window is demonstrated by a third-iteration map. As a result, a type-I intermittent chaos is observed near the periodic window, and occasional irregular bursts will become more frequent as the control parameters move away from the critical point of the saddle-node bifurcation.

ACKNOWLEDGMENT

The research has been financially supported by National Natural Science Foundation of China (Grants No. 12175050 and No. 12205067).

- [1] P. Chu, J. Chen, L. Wang, and N. Huang, Plasma-surface modification of biomaterials, *Mater. Sci. Eng. R* **36**, 143 (2002).
- [2] D. B. Miklos, C. Remy, M. Jekel, K. G. Linden, J. E. Drewes, and U. Hübner, Evaluation of advanced oxidation processes for water and wastewater treatment—a critical review, *Water Res.* **139**, 118 (2018).
- [3] M. Laroussi, Low temperature plasma-based sterilization: Overview and state-of-the-art, *Plasma Proc. Poly.* **2**, 391 (2005).
- [4] Th. von Woedtke, S. Reuter, K. Masur, and K.-D. Weltmann, Plasmas for medicine, *Phys. Rep.* **530**, 291 (2013).
- [5] U. Helmersson, M. Lättemann, J. Bohlmark, A. P. Ehiasarian, and J. T. Gudmundsson, Ionized physical vapor deposition (ipvd): A review of technology and applications, *Thin Solid Films* **513**, 1 (2006).
- [6] N. Frage, S. Kalabukhov, N. Sverdlov, V. Ezersky, and M. P. Dariel, Densification of transparent yttrium aluminum garnet (YAG) by SPS processing, *J. Eur. Ceram. Soc.* **30**, 3331 (2010).
- [7] H. Uchiike and T. Hirakawa, Color plasma displays, *Proc. IEEE* **90**, 533 (2002).
- [8] Z. Chang, C. Wang, and G. Zhang, Progress in degradation of volatile organic compounds based on low-temperature plasma technology, *Plasma Proc. Poly.* **17**, 1900131 (2020).
- [9] Y. P. Raizer and J. E. Allen, *Gas Discharge Physics*, Vol. 1 (Springer, 1991).
- [10] Y. P. Raizer and M. Mokrov, Physical mechanisms of self-organization and formation of current patterns in gas discharges of the Townsend and glow types, *Phys. Plasmas* **20**, 101604 (2013).
- [11] M. Benilov, Multiple solutions in the theory of DC glow discharges and cathodic part of arc discharges. Application of these solutions to the modeling of cathode spots and patterns: A review, *Plasma Sources Sci. Technol.* **23**, 054019 (2014).
- [12] J. Ouyang, L. Ben, H. Feng, and D. Dong, Nonlinear phenomena in dielectric barrier discharges: Pattern, striation and chaos, *Plasma Sci. Tech.* **20**, 103002 (2018).

- [13] T. Fukuyama, R. Kozakov, H. Testrich, and C. Wilke, Spatiotemporal Synchronization of Coupled Oscillators in a Laboratory Plasma, *Phys. Rev. Lett.* **96**, 024101 (2006).
- [14] C. M. Ticos, E. Rosa Jr, W. B. Pardo, J. A. Walkenstein, and M. Monti, Experimental Real-Time Phase Synchronization of a Paced Chaotic Plasma Discharge, *Phys. Rev. Lett.* **85**, 2929 (2000).
- [15] W. X. Ding, H. Q. She, W. Huang, and C. X. Yu, Controlling Chaos in a Discharge Plasma, *Phys. Rev. Lett.* **72**, 96 (1994).
- [16] A. Di Garbo, S. Euzzor, J.-M. Ginoux, F. T. Arcchi, and R. Meucci, Delayed dynamics in an electronic relaxation oscillator, *Phys. Rev. E* **100**, 032224 (2019).
- [17] T. Braun, J. A. Lisboa, R. E. Francke, and J. A. C. Gallas, Observation of Deterministic Chaos in Electrical Discharges in Gases, *Phys. Rev. Lett.* **59**, 613 (1987).
- [18] T. Braun, J. A. Lisboa, and J. A. C. Gallas, Evidence of Homoclinic Chaos in the Plasma of a Glow Discharge, *Phys. Rev. Lett.* **68**, 2770 (1992).
- [19] W. Ding, W. Huang, X. Wang, and C. X. Yu, Quasiperiodic Transition to Chaos in a Plasma, *Phys. Rev. Lett.* **70**, 170 (1993).
- [20] T. Hayashi, Mixed-Mode Oscillations and Chaos in a Glow Discharge, *Phys. Rev. Lett.* **84**, 3334 (2000).
- [21] J. Qin, L. Wang, D. P. Yuan, P. Gao, and B. Z. Zhang, Chaos and Bifurcations in Periodic Windows Observed in Plasmas, *Phys. Rev. Lett.* **63**, 163 (1989).
- [22] E. Pugliese, R. Meucci, S. Euzzor, J. G. Freire, and J. A. Gallas, Complex dynamics of a DC glow discharge tube: Experimental modeling and stability diagrams, *Sci. Rep.* **5**, 8447 (2015).
- [23] Z. L. Petrović and A. V. Phelps, Oscillations of low-current electrical discharges between parallel-plane electrodes. I. dc discharges, *Phys. Rev. E* **47**, 2806 (1993).
- [24] W. X. Ding, H. Deutsch, A. Dinklage, and C. Wilke, Observation of a strange nonchaotic attractor in a neon glow discharge, *Phys. Rev. E* **55**, 3769 (1997).
- [25] T. Price and T. Mullin, An experimental observation of a new type of intermittency, *Physica D* **48**, 29 (1991).
- [26] D. L. Feng, C. X. Yu, J. L. Xie, and W. X. Ding, On-off intermittencies in gas discharge plasma, *Phys. Rev. E* **58**, 3678 (1998).
- [27] S. Chiriac, D. Dimitriu, and M. Sanduloviciu, Type I intermittency related to the spatiotemporal dynamics of double layers and ion-acoustic instabilities in plasma, *Phys. Plasmas* **14**, 072309 (2007).
- [28] D. Dai, H. Hou, and Y. Hao, Influence of gap width on discharge asymmetry in atmospheric pressure glow dielectric barrier discharges, *Appl. Phys. Lett.* **98**, 131503 (2011).
- [29] X. Li, R. Liu, P. Jia, K. Wu, C. Ren, and Z. Yin, Influence of driving frequency on discharge modes in the dielectric barrier discharge excited by a triangle voltage, *Phys. Plasmas* **25**, 013512 (2018).
- [30] X. Li, R. Liu, D. Gong, X. Li, C. Ren, and P. Jia, Influence of external parameters on nonlinear behaviors in a helium dielectric-barrier discharge excited by a modulated voltage, *Phys. Plasmas* **26**, 023514 (2019).
- [31] S. He, J. Ouyang, F. He, and H. Jia, Self-pulsing operating mode of hollow cathode discharge in noble gas, *Phys. Plasmas* **19**, 023504 (2012).
- [32] C. Yuan, C. Yesil, J. Yao, Z. Zhou, and I. Rafatov, Transition from periodic to chaotic oscillations in a planar gas discharge-semiconductor system, *Plasma Sources Sci. Technol.* **29**, 065009 (2020).
- [33] J. L. Walsh, F. Iza, N. B. Janson, and M. G. Kong, Chaos in atmospheric-pressure plasma jets, *Plasma Sources Sci. Technol.* **21**, 034008 (2012).
- [34] D. D. Šijačić, U. Ebert, and I. Rafatov, Period doubling cascade in glow discharges: Local versus global differential conductivity, *Phys. Rev. E* **70**, 056220 (2004).
- [35] C. Yuan, A. Kudryavtsev, A. Saifutdinov, S. Sysoev, J. Yao, and Z. Zhou, Diagnostics of large volume coaxial gridded hollow cathode DC discharge, *Plasma Sources Sci. Technol.* **28**, 067001 (2019).
- [36] Y. Jingfeng, Y. Chengxun, Y. Zhi, Z. Zhongxiang, and A. Kudryavtsev, Measurements of plasma parameters in a hollow electrode AC glow discharge in helium, *Plasma Sci. Technol.* **22**, 034006 (2020).
- [37] Phelps database, www.lxcat.net/phelps.
- [38] S. Euzzor, A. Di Garbo, J.-M. Ginoux, F. T. Arcchi, and R. Meucci, Implementing poincaré sections for a chaotic relaxation oscillator, *IEEE Trans. Circ. Syst. II: Express Briefs* **67**, 395 (2019).
- [39] S. Euzzor, A. Di Garbo, J.-M. Ginoux, S. Zambrano, F. Arcchi, and R. Meucci, On the destabilization of a periodically driven three-dimensional torus, *Nonlinear Dyn.* **103**, 1969 (2021).
- [40] J.-M. Ginoux, R. Meucci, S. Euzzor, and A. Di Garbo, Torus breakdown in a uni junction memristor, *Int. J. Bifur. Chaos* **28**, 1850128 (2018).